CHEMISTRY

*i*PP/HDPE blends compatibilized by a polyester: An unconventional concept to valuable products

Jakub Kruszynski[1,2]†, Weronika Nowicka[1,2]†, Artur Rozanski[3], Yingxin Liu[1], Daniele Parisi[4], Lanti Yang[5], Farhan Ahmad Pasha[6], Miloud Bouyahyi[1], Lidia Jasinska-Walc[1,2]*, Rob Duchateau[1,4]*

Polyolefins are the most widely used plastics accounting for a large fraction of the polymer waste stream. Although reusing polyolefins seems to be a logical choice, their recycling level remains disappointingly low. This is mainly due to the lack of large-scale availability of efficient and inexpensive compatibilizers for mixed polyolefin waste, typically consisting of high-density polyethylene (HDPE) and isotactic polypropylene (*i*PP) that, despite their similar chemical hydrocarbon structure, are immiscible. Here, we describe an unconventional approach of using polypentadecalactone, a straightforward and simple-to-produce aliphatic polyester, as a compatibilizer for *i*PP/HDPE blends, especially the brittle *i*PP-rich ones. The unexpectedly effective compatibilizer transforms brittle *i*PP/HDPE blends into unexpectedly tough materials that even outperform the reference HDPE and *i*PP materials. This simple approach creates opportunities for upcycling polymer waste into valuable products.

INTRODUCTION

With a market share of more than 60% and having the lowest lifecycle environmental impact of all polymers, polyolefins play a crucial role in our daily life (*1*–*5*). Polyolefins are lightweight, cheap, and food contact–approved, which makes them materials of choice for, often single-use, packaging applications and other fast-moving consumer goods. Consequently, vast amounts of polyolefin waste are produced annually. Driven by environmental awareness concerning the pollution of polymer waste and the carbon footprint of single-use plastics, a growing amount of these polyolefins end up in recycle streams rather than being landfilled or incinerated. Recycled polyolefin waste can be separated relatively easily from other polymers based on their density. However, separating polyolefins from each other is challenging (*6*, *7*). The purity levels of current post-consumer recycle polyolefins, consisting of high-density polyethylene (HDPE) and isotactic polypropylene (*i*PP), range between 80 and 90% of either HDPE or *i*PP. Although this level of purity might seem adequate for mechanical recycling, the bulk properties, especially the *i*PP-rich blends, are rather disappointing (*8*). Despite both being simple aliphatic hydrocarbons, blends of HDPE and *i*PP are immiscible forming distinct phases (*9*). To overcome the resulting poor mechanical properties, various compatibilizer strategies have been developed including miscibility and interfacial properties studies in ternary blends (*10*–*12*). The most common compatibilizers are block or graft copolymers consisting of HDPE and *i*PP segments (*13*–*23*). A major breakthrough in this field was achieved by Coates and coworkers, who demonstrated that small amounts of an HDPE- and *i*PP-based tetrablock copolymer ensure the exceptional performance of HDPE/*i*PP blends and laminates (*24*).

Despite the promising results of using block and graft copolymers as compatibilizers, their synthesis is challenging and often costly, which encumbers their large-scale production and widespread use. To accommodate the recycling of the vast and ever-growing amounts of mixed polyolefin waste produced yearly, cheap and easy-to-synthesize compatibilizers will be essential.

We envisioned an unconventional complementary strategy to compatibilize *i*PP/HDPE blends based on the concept of finding an inexpensive and easy-to-produce homopolymer that has a clear affinity for both HDPE and *i*PP. Although finding a homopolymer to effectively compatibilize HDPE/*i*PP blends seems very unlikely, the literature provides several interesting leads. Long-chain aliphatic polyesters have shown remarkable PE-like properties (*25*–*27*). Polypentadecalactone (PPDL), for example, has a crystal structure, unit cell parameters, and properties similar to those of HDPE (fig. S1). Although still immiscible, PPDL and HDPE form blends with excellent mechanical properties, which find their origin in the epitaxial crystallization of PPDL onto HDPE, resulting in lamellae penetration through the interface of the two polymers (*28*). The affinity of PPDL for *i*PP has thus far never been studied.

Pentadecalactone (PDL) is a renewable product that belongs to the class of naturally occurring macrocyclic musks used in the fragrance industry. Its eco-friendliness led to an increased demand and the development of improved synthetic routes, which makes PDL commercially available in larger quantities (*29*). PDL can conveniently be polymerized using catalytic ring-opening polymerization to afford PPDL, a linear aliphatic polyester having 14 CH_2 moieties between each ester group (*30*–*32*). The combination of an inexpensive catalyst and low polymerization temperature renders this chain growth polymerization process sustainable and scalable using standard melt polymerization reactors. For this study, a PPDL with $M_n = 99.5$ kg mol^{-1} and $Đ = 2.2$ was synthesized.

RESULTS AND DISCUSSION

To investigate whether PPDL also shows affinity to *i*PP and hence might function as a compatibilizer for blends consisting of HDPE and *i*PP, molecular dynamics simulations were performed. The miscibility of polymer blends is typically described by miscibility parameters

[1]SABIC Technology & Innovation, STC Geleen, Urmonderbaan 22, Geleen, Netherlands. [2]Department of Chemistry and Technology of Functional Materials, Chemical Faculty, Gdansk University of Technology, G. Narutowicza Str. 11/12, 80-233 Gdansk, Poland. [3]Centre of Molecular and Macromolecular Studies, Polish Academy of Sciences, Sienkiewicza 112, 90-363 Lodz, Poland. [4]Chemical Product Engineering, Department of Chemical Engineering, University of Groningen, Nijenborgh 4, 9747 AG Groningen, Netherlands. [5]SABIC Technology & Innovation, Plasticslaan 1, 4612 PX, Bergen op Zoom, Netherlands. [6]SABIC Technology Center at KAUST, 25 Unity Blvd, Thuwal 23955, Saudi Arabia.
*Corresponding author. Email: lidia.jasinska-walc@sabic.com (L.J.-W.); rob.duchateau@sabic.com (R.D.)
†These authors contributed equally to this work.

such as the binding energy ($E_{binding}$), mixing energy (ΔE_{mix}), and the Flory-Huggins interaction parameter (χ). These parameters depend on the Hildebrand solubility parameter (δ) and cohesive energy densities (CEDs) (*33*–*35*), which can be obtained from molecular dynamics simulations (*36*–*40*). For the simulations of the *i*PP/HDPE blends (with and without PPDL as compatibilizer), four models with different *i*PP and HDPE ratios were used (Fig. 1). The models PP′ ($PP_{82.3wt\%}/HDPE_{9.7wt\%}/PPDL_{8.0wt\%}$) and PP″ ($PP_{74.6wt\%}/HDPE_{18.1wt\%}/PPDL_{7.3wt\%}$) represent *i*PP-rich blends, while PE′ ($PP_{12.4wt\%}/HDPE_{73.1wt\%}/PPDL_{14.5wt\%}$) and PE″ ($PP_{10.0wt\%}/HDPE7_{8.3wt\%}/PPDL_{11.7wt\%}$) reflect the HDPE-rich compositions (Fig. 1E). To exclude crystallization-related phenomena, all the modeling was performed at 190°C as the processing temperature of the blends. First, the miscibility of binary *i*PP/PPDL, HDPE/PPDL, and *i*PP/HDPE blends (~90:10 w/w) were investigated (Fig. 1C, figs. S2 to S4, and table S1). Furthermore, PPDL—like other long-chain aliphatic polyesters, thoroughly studied by Mecking and coworkers (*41*)—and HDPE are structurally the most similar polymers; the $E_{binding}$ is the lowest of all three binary blends. The $E_{binding}$ for the *i*PP/PPDL blend is significantly higher than for the HDPE/PPDL blend, which, based on the molecular structure of the polymers, was not expected. The higher affinity of *i*PP to PPDL than to HDPE was underlined by the higher $E_{binding}$ for the *i*PP/PPDL as compared to the corresponding *i*PP/HDPE blend. The corresponding ΔE_{mix} and χ parameters show the same trend. These encouraging results incited us to study whether or not PPDL would have a compatibilizing effect on *i*PP/HDPE blends (Fig. 1, figs. S5 and S6, and table S2). *i*PP/HDPE blends are immiscible at room temperature, leading to a positive Flory-Huggins interaction parameter (χ) (*40*, *42*–*44*) at room temperature. However, these simulations were performed at 190°C (processing temperature), and at this temperature, the molten mixture of iPP/HDPE shows a negative Flory-Huggins interaction parameter (χ), as depicted in Fig. 1C. The *i*PP/HDPE/PPDL ternary blends show a more negative (χ) value in all the cases in comparison to respective binary *i*PP/HDPE mixtures. This qualitative trend demonstrates that the presence of PPDL increases miscibility. Figure 1B shows a strong increase (nearly doubling) of the $E_{binding}$ upon the addition of PPDL to each of the blends, which demonstrates the compatibilizing capability of PPDL in all of these systems. The $E_{binding}$ is considerably higher for the *i*PP-rich blends compared to the HDPE-rich blends, being in agreement with the abovementioned higher affinity of PPDL for *i*PP than for HDPE. To understand the origin of the difference in $E_{binding}$ iPP/PPDL and HDPE/PPDL, a detailed study on the complex relationships between chain, molecular and topological aspects, structure, morphology, and properties will be required, which falls out of the scope of the current work. The best compatibilizing effect is found for the PP″ blend (*i*PP/HDPE w/w ratio is 80/20; *i*PP/HDPE/PPDL w/w/w ratio is 75/18/7). The ΔE_{mix}, derived from the CED and fractional volume of the individual components, shows a very similar trend as the $E_{binding}$ and is the lowest for *i*PP-rich blends, especially for PP″ (Fig. 1D). The Flory-Huggins interaction parameter also shows the most negative value for the compatibilized *i*PP-rich blend PP″ (Fig. 1C). The literature on solubility parameters such as $E_{binding}$, mixing energy (ΔE_{mix}), and the Flory-Huggins interaction parameter (χ) for HDPE/iPP is scattered, and to our best knowledge, we could not find these values at 190°C (processing temperature) for HDPE/iPP to adjudge the quantitative reliability. Nevertheless, the calculated values are good qualitative indications for these HDPE/iPP/PPDL mixtures, which encouraged us to experiment investigation of PPDL potential as a compatibilizer for HDPE/*i*PP blends of different compositions.

To obtain more detailed insight into the interactions between PPDL, HDPE, and *i*PP, wide-angle x-ray scattering (WAXS) analysis of the individual blend components has been performed and thermal properties, as well as the morphology of the binary blends, have been studied by differential scanning calorimetry (DSC) and transmission electron microscopy (TEM) analysis, respectively. The blends were prepared in a corotating twin screw extruder and analyzed by size exclusion chromatography (SEC) (fig. S7 and table S3). The WAXS profiles show a clear resemblance of the orthorhombic crystal structures of PPDL and HDPE, whereas *i*PP crystallizes in the monoclinic α form (Fig. 2, A and B, and fig. S1) (*45*). The individual components in the blends crystalize independently and do not affect each other (*46*). DSC analysis (Fig. 2C and fig. S8) revealed that blending HDPE with PPDL leads to a substantial increase in the crystallization temperature (T_c) of PPDL by 5°C. This behavior can be explained by the aforementioned epitaxial crystal growth of PPDL onto HDPE lamellae, which function as nucleating agents (*28*). Conversely, no increase in T_c of PPDL is observed upon blending with *i*PP, which is in agreement with the lack of epitaxy for this system. However, the T_c of *i*PP increased substantially from 113° to 121°C when mixed with PPDL, which is likely a result of heterogeneous nucleation caused by spinodal decomposition leading to a reduced nucleation barrier (*47*). TEM spectroscopy confirms that epitaxy, usually accompanied by clear lamellae penetration through the interface of immiscible components, is the origin of the affinity between HDPE and PPDL (Fig. 2, D and E) (*28*, *48*). As a result, the HDPE/PPDL blend image does not reveal a clear interphase between the PPDL and HDPE matrix. On the other hand, the morphological study of the *i*PP/PPDL blend exhibited a pronounced phase separation of the components with no indication of epitaxy for *i*PP/PPDL blends. However, a rather rough interphase does suggest some partial mixing of the amorphous phase at the interface. Hence, both molecular dynamics simulations and experimental data demonstrate that PPDL has an affinity to both HDPE and *i*PP, albeit different in nature. Whereas the resemblance in the crystal structure of PPDL and HDPE results in epitaxy, PPDL and *i*PP show better miscibility of the amorphous phases.

The next step was to experimentally test the efficiency of PPDL as a compatibilizer for *i*PP/HDPE blends. As mentioned earlier, most *i*PP and HDPE recycle streams contain more than 80% of the main components. Whereas HDPE-rich recycled materials reveal good mechanical properties, the mechanical performance of the *i*PP-rich congeners is unsatisfactory due to their brittle nature. We therefore focused on *i*PP-rich blends and used compositions with 80/20 and 90/10 *i*PP/HDPE w/w ratios.

First, the thermal properties (fig. S9 and table S4) and morphologies (Fig. 3 and figs. S10 to S12) of the ternary *i*PP/HDPE/PPDL blends were investigated. The *i*PP/HDPE/PPDL 90/10/5 and 80/20/5 w/w/w compositions show the same increase (5°C) in the T_c of the PPDL as for the binary HDPE/PPDL blend. The T_c of *i*PP also increases for both blends, but less as compared to the *i*PP/PPDL blend (4°C versus 8°C). Most likely, the crystallization of HDPE results in heterogeneous nucleation of the *i*PP (*49*, *50*). The presence of distinct PPDL crystallization and melting peaks indicates that, upon cooling, even a small amount of PPDL forms a separated phase in the blends. The comparison of the TEM images of the *i*PP/HDPE 90/10 w/w and *i*PP/HDPE/PPDL 90/10/5 w/w/w compositions reveals a substantial decrease of the HDPE domain size from an average of 400 to 200 nm upon the addition of PPDL, indicative for the compatibilizing effect of the latter (Fig. 3, A and B, and fig. S10). Although the HDPE is well

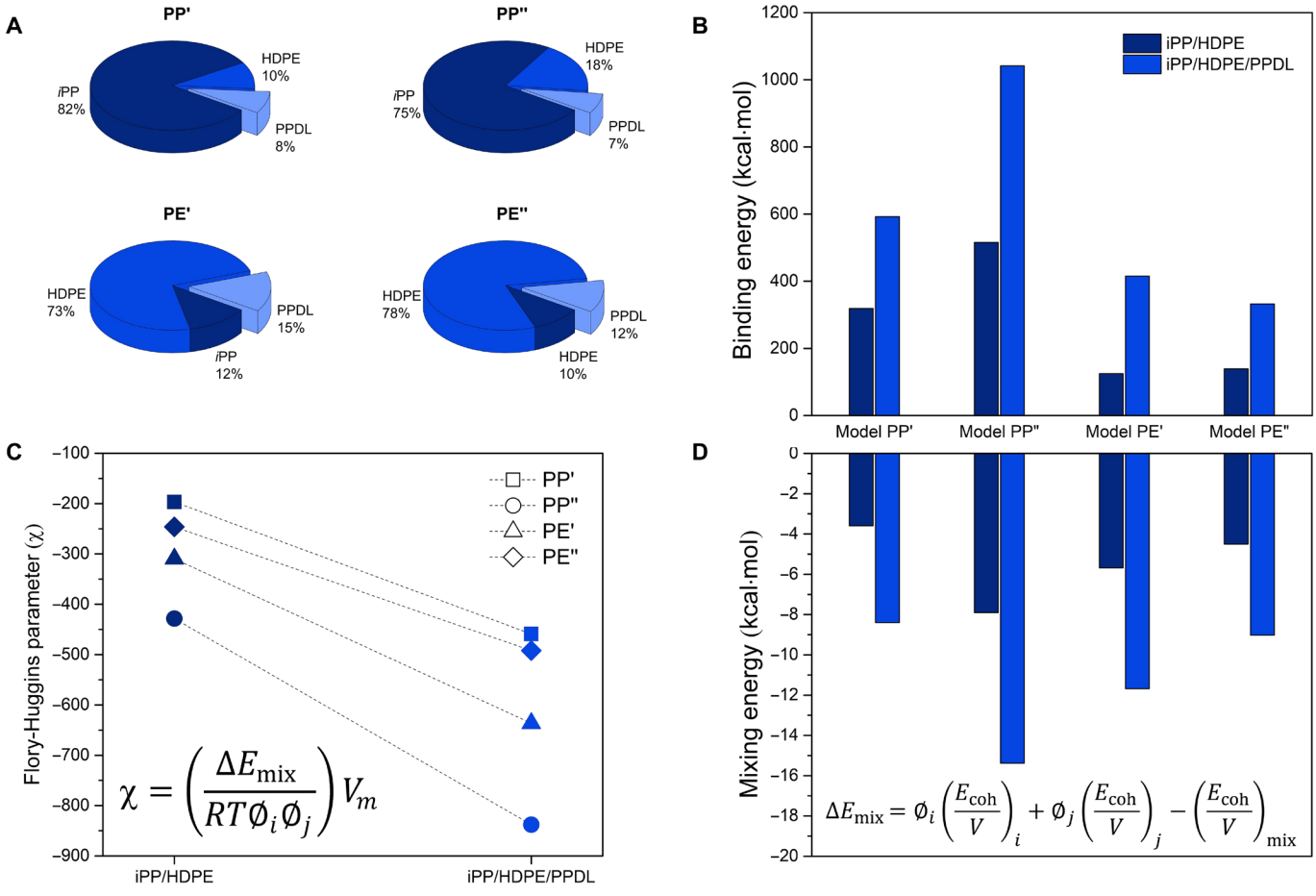

E

Blend component	Model PP'	Model PP''	Model PE'
iPP (wt %)	82.3	74.6	12.4
HDPE (wt %)	9.7	18.1	73.1
PPDL (wt %)	8.0	7.3	14.5
HDPE/iPP ratio	11:89	20:80	85:15
iPP chains	12	12	1
HDPE chains	18	37	75
PPDL chains	2	2	2

Fig. 1. Molecular Dynamics simulation of polymer miscibility. Blend compositions (**A**), binding energy E_{binding} (**B**), Flory-Huggins interaction parameter χ (**C**), and mixing energy E_{mix} (**D**) for noncompatibilized and compatibilized blends PP′, PP″, PE′, and PE″ as well as input data for modeling (**E**).

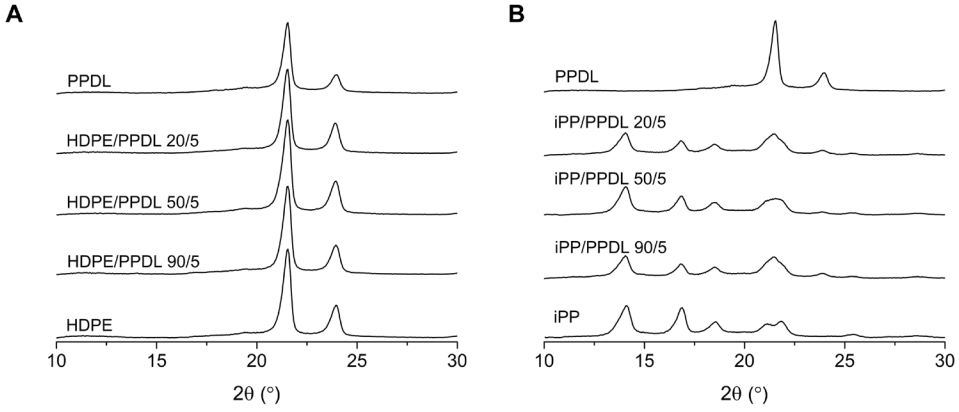

C

Sample	T_m °C	T_c °C	ΔH_m J·g
*i*PP	161.4	113.5	74.8
HDPE	131.1	118.5	180.5
PPDL	94.7	79.0/33.1	108.7
*i*PP/PPDL 90/5	162.8/93.0	121.0/79.7	90.4/4.0
*i*PP/PPDL 50/5	162.3/93.6	119.0/80.3	79.7/12.0
*i*PP/PPDL 20/5	162.3/93.8	120.3/80.6	84.3/16.9
HDPE/PPDL 90/5	129.7/93.2	117.9/84.5	149.4/3.4
HDPE/PPDL 50/5	130.5/93.7	117.2/84.2	151.4/5.5
HDPE/PPDL 20/5	129.5/93.6	117.5/84.5	127.3/14.4

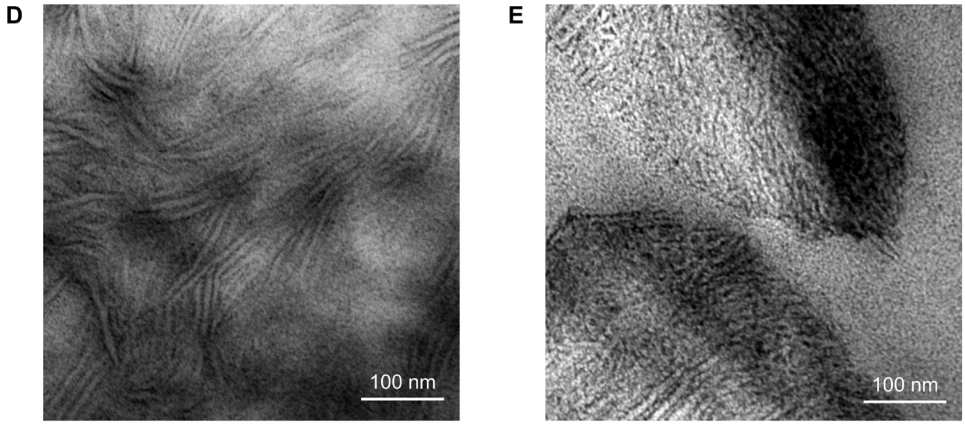

Fig. 2. Morphology and thermal analysis of HDPE/PPDL and *i*PP/PPDL blends. WAXS analysis HDPE/PPDL, *i*PP/PPDL, and individual polymers used for their preparation (**A** and **B**), thermal properties of the HDPE/PPDL, *i*PP/PPDL blends, and individual polymers used for their preparation analyzed by DSC (**C**), TEM analysis of HDPE/PPDL (**D**), and *i*PP/PPDL (**E**) 90/10 w/w blends.

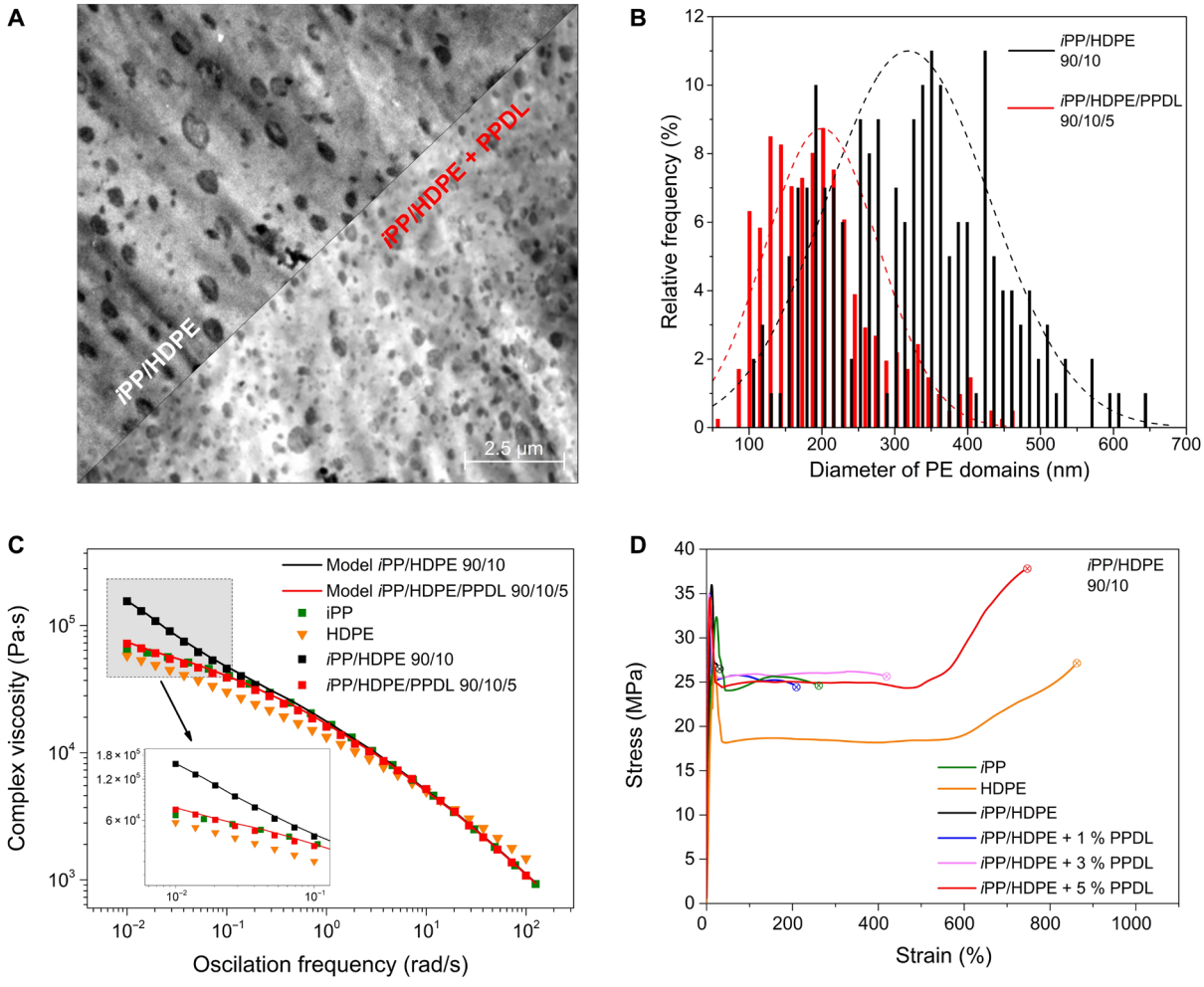

Fig. 3. Morphology and performance analysis of *i*PP/HDPE 90/10 w/w blends. TEM image of the *i*PP/HDPE 90/10 w/w blend and *i*PP/HDPE/PPDL 90/10/5 w/w/w blend (**A**). The compatibilizing effect of PPDL visualized by HDPE-dispersed phase size determination in *i*PP/HDPE and *i*PP/HDPE/PPDL blends using TEM (**B**). Measured (symbols) and calculated (line) complex viscosity (η*) of *i*PP, HDPE, uncompatibilized *i*PP/HDPE 90/10 blend, and compatible *i*PP/HDPE/PPDL 90/10/5 composition. Samples were tested under oscillation frequency (ω) at a constant temperature of 190°C (**C**). Static mechanical properties measurements of the compatibilized *i*PP/HDPE/PPDL blend, the uncompatibilized *i*PP/HDPE blend, and *i*PP, HDPE, and PPDL reference materials (**D**).

dispersed, a slightly less pronounced reduction of the HDPE domain sizes has been observed for the *i*PP/HDPE/PPDL 80/20/5 w/w/w blend compared to the uncompatibilized *i*PP/HDPE 80/20 w/w blend (figs. S11 and S12). This might originate from an insufficient amount of compatibilizer with respect to the contribution of HDPE in the final product. For both blends, the presence of PPDL leads to a significant change in the interphase between the blend components, which allows HDPE lamellae penetration into the *i*PP matrix (figs. S10 and S11).

Atomic force microscopy (AFM) quantitative nanomechanical mapping (QNM) was applied for a quantitative mapping of the blends' nanomechanical properties (figs. S13 and S14). Peak-force QNM, used for the modulus mapping of the blends' components, revealed two well-defined *i*PP and HDPE phases for the uncompatibilized *i*PP/HDPE 90/10 w/w blend with an elastic modulus of 2.5 ± 0.2 GPa and 1.7 ± 0.2 GPa, respectively. It is important to underline that, typically, the viscoelastic responses of polymer samples are frequency dependent and an increase of the storage modulus and the glass transition temperature might be observed at higher frequencies (*51*). AFM-QNM analyses performed at a frequency of 2000 Hz, which is 1000 times higher than the typical bulk mechanical testing by DMTA analysis, demonstrate slightly higher modulus values for both the *i*PP and the HDPE phase in the tested blend sample in comparison to the DMA results performed at orders lower frequency (*52*). The addition of PPDL to the *i*PP/HDPE 90/10 w/w composition did not seem to have a significant effect on the *i*PP (2.5 ± 0.2 GPa to 2.2 ± 0.2 GPa) and HDPE (1.7 ± 0.2 GPa to 1.3 ± 0.2 GPa) moduli as the values are indistinguishable within the error on the measurement. A similar result was obtained for the *i*PP/HDPE/PPDL 80/20/5 w/w/w composition. Whereas no drop in glass transition temperature [T_g, determined using dynamic mechanical thermal analysis (DMTA)] was observed for the ternary blends *i*PP/HDPE/PPDL, the lower T_g values of binary iPP/PPDL and HDPE/PPDL blends suggest a plasticizing effect for these blends (figs. S15 to S18 and table S5). The incorporation of increasing quantities of PPDL into *i*PP resulted in a reduction of the T_g from 7° to 3°C, being

in agreement with the theoretical values calculated using the Flory-Fox equation (see the Supplementary Materials: discussions concerning compatibilizer distribution in the blends). In addition, above the glass transition temperatures, only a minor decrease in the *i*PP storage and loss moduli was observed, indicating a small impact of PPDL on the viscoelastic properties of the polypropylene, as also proven by AFM-QNM. The storage and loss moduli of the *i*PP/HDPE blends compatibilized by PPDL maintain the desired performance characteristics, ensuring the suitability of the blends for high-temperature applications designed for *i*PP.

The effect of the PPDL compatibilizer on *i*PP/HDPE 90/10 w/w blends was also assessed by means of shear rheology in the linear viscoelastic regime (Fig. 3C). The two pure components, *i*PP and HDPE, exhibit a quantitatively similar flow curve, characterized by the onset of a Newtonian regime, and a well-resolved shear thinning region with a slope between 0.7 and 0.8, in agreement with past works on melts, in particular, polydisperse *i*PPs (*53*). The uncompatibilized *i*PP/HDPE 90/10 w/w blend yielded a rheological spectrum that displays a low-frequency viscosity upturn that sets the blend far from Newtonian behavior, reflecting poor miscibility and the presence of agglomerates which prevents flow behavior. Conversely, the *i*PP/HDPE 90/10 blend compatibilized with 5% PPDL shows Newtonian behavior at low frequencies and a slightly higher viscosity compared to the reference *i*PP (see inset of Fig. 3C). That is, the presence of PPDL allowed for a blend, with the intact shear thinning region, relevant for the processability of the polymers. The model of Gramespacher and Meissner (G-M) was adopted to capture the experimental rheological observations and highlight the effect of the PPDL on the blends (*54*). The G-M model is based on the additive contributions to the complex shear modulus of the continuous and dispersed phases, as well as the polymer interface. The latter is a function of the average domain size of the dispersed domains, and the interfacial energy. Note that the linear mixing rule works well when the blend constituents have Newtonian viscosities of the same order of magnitude, as in the present case (*54*). For the noncompatibilized blend, an average domain size of 318.5 nm taken from Fig. 3B and typical interfacial energy for *i*PP/HDPE blends of 1.6 mN/m were adopted (*55*). With such parameters, the model well-described the observed data (see black line in Fig. 3C). For the compatibilized blend, with an average domain size of 200 nm taken from Fig. 3B, the best fit of the data was obtained with a lower interfacial energy equal to 0.1 mN/m. The result of this model corroborates the hypothesis that PPDL lowers the interfacial energy between the investigated polyolefins.

Although molecular dynamics simulations, physical properties analyses, and morphological studies strongly indicate that PPDL functions as a compatibilizer for HDPE/*i*PP blends, the ultimate proof is provided by a static mechanical properties study (Fig. 3D, Table 1, figs. S19 and S20, and table S6). Pristine *i*PP and HDPE display ductile behavior when exposed to external uniaxial tension, which, for the grades used in our study, resulted in an average elongation at break of 290 and 930%, respectively. With stress (273 MPa) and strain (1050%) at the break, the tensile behavior of PPDL strongly resembles that of HDPE. Conversely, the brittle failure with a maximum strain at a break of only 32% of the uncompatibilized *i*PP/HDPE blends is illustrative of their poor mechanical performance. The addition of a small amount of PPDL, miscible with *i*PP, epitaxially crystalizing onto HDPE and partially localized at the interphase (figs. S21 and S22), appeared to have a profound and unexpected effect on the mechanical properties of this blend. Unexpectedly, the strain at the break values for both compatibilized *i*PP/HDPE/PPDL 90/10/5 and 80/20/5 w/w/w blends (726 and 656%, respectively) did not only approach that of pristine *i*PP, as was hoped, but they are even more than two times higher than the value for *i*PP and are close to the strain at the break of HDPE. In addition, a strain hardening comparable to HDPE provides a significant enhancement of the stress at break from 23 to 32 MPa. The addition of 5% of PPDL does not lead to a decrease in the yield stress or modulus. As a result, the addition of a small amount of PPDL transforms the brittle uncompatibilized *i*PP/HDPE blend into a material with a considerably increased toughness than pristine *i*PP and HDPE. In the interest of optimizing the compatibilizer amount, *i*PP/HDPE compositions containing 3 and 1 wt % of PPDL were also tested (fig. S20 and table S6). Lowering the amount of PPDL from 5 to 3 wt % and lastly to 1 wt % leads to a gradual drop of the stress and strain at break. But even with 1 wt % of PPDL in the blend, a strain at break similar to that of a neat *i*PP is obtained. It is worth mentioning that injection-molded specimens revealed improved mechanical properties as the compression-molded counterparts (fig. S19 and table S6), clearly proving the potential for large-scale industrial application of

Table 1. Static mechanical properties of the *i*PP/HDPE, *i*PP/HDPE/PPDL blends, and polymers used for their preparation.

Sample	Yield stress MPa	Yield strain %	Stress at the break MPa	Strain at the break %
*i*PP	34.7 ± 1.8	13.5 ± 3.4	20.5 ± 2.2	292 ± 121
HDPE	28.9 ± 1.4	11.1 ± 2.8	23.2 ± 5.5	934 ± 123
PPDL	19.1 ± 0.8	9.7 ± 1.8	27.3 ± 2.0	1050 ± 116
*i*PP/HDPE 90/10	34.8 ± 1.3	11.7 ± 1.7	23.0 ± 8.3	32 ± 25
*i*PP/HDPE 80/20	33.9 ± 0.8	9.1 ± 1.8	21.8 ± 9.9	26 ± 18
iPP/HDPE/PPDL 90/10 + 1% PPDL	34.3 ± 0.5	6.6 ± 0.3	19.2 ± 10.5	289 ± 238
iPP/HDPE/PPDL 90/10 + 3% PPDL	34.9 ± 0.6	6.0 ± 0.2	28.2 ± 10.9	464 ± 191
*i*PP/HDPE/PPDL 90/10 + 5% PPDL	34.5 ± 0.4	8.3 ± 0.5	31.7 ± 8.6	726 ± 127
*i*PP/HDPE/PPDL 80/20 + 5% PPDL	34.5 ± 0.8	7.6 ± 0.6	24.0 ± 10.4	656 ± 146

this approach to compatibilizing *i*PP/HDPE blends with a simple polyester-like PPDL.

We have demonstrated that a simple-to-produce aliphatic polyester can function as a highly effective compatibilizer for otherwise brittle, low-value *i*PP/HDPE blends. The origin of the compatibilizing effect of PPDL for *i*PP/HDPE blends is twofold in nature. PPDL reveals epitaxial growth from HDPE lamellar crystals and miscibility with the amorphous phase of *i*PP. PPDL-compatibilized *i*PP-rich blends are characterized by a decrease of the HDPE domain size from 400 to 200 nm, an increase of the T_c of PPDL due to epitaxy, and a reduced T_g of the *i*PP phase due to the partial miscibility of the amorphous phases of PPDL and *i*PP. The static mechanical properties of the PPDL-compatibilized *i*PP/HDPE blends are exceptional showing a strong toughening effect of PPDL on the *i*PP/HDPE blend. The unexpectedly effective compatibilizer transforms brittle *i*PP/HDPE blends into unexpectedly tough materials that even outperform the reference HDPE and *i*PP materials. Its simplicity makes this approach easily scalable and unlocks a potential route to convert large amounts of mixed polyolefin waste into high added value, high-volume products.

MATERIALS AND METHODS

Materials

Isotactic PP (PP531PH grade, received from SABIC), HDPE (HDPE B5429 grade, received from SABIC), Irganox 1010 (purchased from BASF), ω-pentadecalactone (PDL, >97%), benzyl alcohol (99.8%), calcium hydride (>97%), $Al(CH_3)_3$ (2 M solution in toluene) purchased from Merck, *N*,*N*′-bis(salicylidene)-2,2-dimethyl-1,3-propanediamine (98%, purchased from Sigma-Aldrich) and dry ethanol (purchased from Biosolve) were all used as received. Tetrahydrofuran and toluene (purchased from Sigma-Aldrich) were dried using an MBraun-SPS-800 purification column system.

Synthesis of Salen aluminum methyl

In a nitrogen-filled MBraun glove box, a toluene solution of *N*,*N*′-bis (salicylidene)-2,2-dimethyl-1,3-propanediamine (Salen ligand; 0.4 M, 20 mmol, 50 ml) was added to a toluene solution (0.5 M, 10 mmol, 20 ml) of trimethyl aluminum. After 1 hour, the Schlenk flask was taken out of the glove box and the pale yellow mixture was heated to 100°C for 2 hours after which the solvent was removed in vacuo leaving Salen aluminum methyl as an off-white solid in quantitative yield.

Synthesis of PPDL

In a nitrogen-filled MBraun glove box, the Salen aluminum methyl precatalyst (97.2 mg, 0.28 mmol) was dissolved in toluene (4.0 g) and treated with benzyl alcohol (22.5 mg, 0.21 mmol). The glass crimp cap vial containing the clear catalyst solution was tightly closed and removed from the glove box. The catalyst solution was introduced by syringe into a steel reactor charged with molten PDL (50 g, 0.208 mol). The reactor content was stirred (300 rpm) using a magnetic stirrer and heated (140°C) using a heating plate for 24 hours. Then, the product was removed from the reactor, washed with methanol, and dried in a vacuum oven at 50°C for 48 hours.

Preparation of iPP/HDPE, iPP/HDPE/PPDL, iPP/PPDL, and HDPE/PPDL blends

All blends were prepared using exactly the same procedure, only differing in the amounts of *i*PP, HDPE, and PPDL. The appropriate amounts of blend components (approximately 40 g in total) were measured, mixed with antioxidant Irganox 1010 [2500 parts per million (ppm)], and fed into a corotating twin-screw extruder heated to 190°C and a screw rotation rate set at 120 rpm resulting in a residence time of 1.5 min. To ensure good mixing, each mixture was passed two times through the extrusion.

Typical procedure for the preparation of an iPP/HDPE/PPDL blend

*i*PP (PP531PH, 36 g), HDPE (HDPE B5429, 4 g), and PPDL (2 g) with antioxidant Irganox 1010 (2500 ppm) were fed into a corotating twin-screw extruder. The extruder temperature was set at 190°C and the screw rotation rate was set at 120 rpm. The mixture was extruded two times with an average residence time of 1.5 min.

Typical procedure for the sample preparation via injection molding

After blending in the extruder, the mixture was evacuated directly to a mini-injection molding machine with a stainless steel mold in accordance with ISO 527-3, type 5A. The injection temperature was set at 190°C, and the process took place under a pressure of 15 MPa.

Typical procedure for the sample preparation via compression molding

Compression molding of the polymer blends was performed using PP ISO settings on a LabEcon 600 high-temperature press (Fontijne Presses, The Netherlands). The materials were introduced into a Teflon mold to prepare samples with a thickness of 1 mm. The program for the compression molding involved the following steps: heating to 190°C for 5 min under 100-kN force followed by cooling to room temperature for 10 min under applied force.

Methods

Molecular dynamics model preparation

To create a realistic model, we used the number of average molecular weights of the HDPE (M_n = 13.0 kg mol^{-1}), *i*PP (M_n = 166.9 kg mol^{-1}), and PPDL (M_n = 99.5 kg mol^{-1}) that were actually used in blending experiments in this study. The molecular weights needed to be normalized by a factor of 10 resulting in HDPE, *i*PP, and PPDL chains consisting of 47, 400, and 40 monomeric units, respectively (Fig. 1). All molecular dynamics simulations were performed in the process temperature at which the polymers were blended experimentally (190°C). This temperature was also chosen to avoid problems due to the semicrystalline nature of all three polymers. On the basis of calculations and experimental data, the density of 0.76 g cm^{-3} was selected for the polymer mixtures (*56*).

The simulations were performed using BIOVIA Materials Studio 2022 (*57*). The Amorphous Cell module was used to construct representative models of the different polymer mixtures (*58*). The Forcite module was used for periodic boundary condition-based molecular dynamics calculations to predict key properties. The most advanced condensed-phase optimized molecular potentials for atomistic simulations studies (COMPASSIII) was selected for the molecular dynamics simulations (*59*–*62*). In COMPASSIII, the total energy (E_{total}) of the simulation system is represented by the summation and nonbonding interactions (Eqs. 1 and 2).

$$E_{total} = E_b + E_q + E_{\emptyset} + E_{\chi} + E_{cross} + E_{vdw} + E_{ele} \quad (1)$$

$$E_{total} = E_{valence} + E_{cross} + E_{nonbond} \quad (2)$$

Four different models with different *i*PP and HDPE ratios were used. The models PP′ and PP″ are *i*PP-rich, while PE′ and PE″ are HDPE-rich. A detailed description of these models is covered in table S2 and the models are depicted in Fig. 1 and fig. S5. Each set's constructed three-dimensional cubic cell was subjected to a series of

geometry optimization and molecular dynamics simulations using a Forcite module as implemented in Materials Studio 2022. First, the cell was annealed with a periodic boundary condition to 190°C for 0.5 ps with a pressure of 10^{-3} GPa to eliminate internal stress. Subsequently, the cells were subjected to equilibration: First, the geometry was optimized using the smart method (including steepest descent, conjugate gradient, and the Newton method) for more than 10^5 steps until a convergent value was reached. Then, the cubic cells were refined by ultrashort molecular dynamics *NVT* (constant number of particles, *N*, volume, *V*, and temperature, *T*) simulation equilibrated at 190°C with a time step of 0.5 fs for 5000 steps followed by an *NPT* ensemble run at 190°C with a time step of 0.5 fs for 30,000 steps. Minimum fluctuations in density and energy were two cutoff criteria to determine the equilibrium of the system. Last, the equilibrated cells were subjected to a production run of *NPT* (constant number of particles, pressure, and temperature) ensemble at 190°C for 1000 ps. The miscibility parameters such as binding energy ($E_{binding}$), mixing energy (ΔE_{mix}), and Flory-Huggins interaction parameter (χ) were calculated for all four models and respected values are reported in table S2. The energy versus time maps of all four models are depicted in fig. S6. From fig. S6, it can be concluded that the energy of the system shows a minute fluctuation at approximately the average value, indicating that the systems are in an equilibrium state. Once the cubic cells of the ternary blends $PP'_{(PP/HDPE/PPDL)}$, $PP''_{(PP/HDPE/PPDL)}$, $PE'_{(PP/HDPE/PPDL)}$, and $PE''_{(PP/HDPE/PPDL)}$ were constructed, they were used to construct and analyze the corresponding binary blends $PP'_{(PP/HDPE)}$, $PP'_{(PP/PPDL)}$, and $PP'_{(HDPE/PPDL)}$. To be consistent in sample volume, the third components of the original ternary blends were removed and the density of the remaining two components was taken as variable.

The conceptual basis of calculated properties

Hildebrand solubility parameter (δ). Hildebrand solubility parameter (δ) may be calculated by the square root of the CED as shown in Eq. 3 and describes the attractive strength between the molecules of the material (Eq. 4), exerting a huge influence on blend miscibility

$$\delta = \sqrt{\mathrm{CED}} \tag{3}$$

$$\delta_{T^2} = \delta_{vdw^2} + \delta_{ele^2}, \delta_{ele^2} = \delta_{H^2} + \delta_{P^2} \tag{4}$$

The CEDs are known to vary considerably with the molecular weight of the polymer. If all intramolecular forces are eliminated, CED is defined (Eq. 5) as the increase in energy per mole of a material (*33*, *34*)

$$\mathrm{CED} = \left({}^{E_{coh}}/_{V} \right) \tag{5}$$

Mixing energy. The computational results of CED allow the calculation of the energy of mixing, ΔE_{mix} (*38*), of a binary mixture of components *i* and *j* according to Eq. 6

$$\Delta E_{mix} = \emptyset_i \left(\frac{E_{coh}}{V} \right)_i + \emptyset_j \left(\frac{E_{coh}}{V} \right)_j - \left(\frac{E_{coh}}{V} \right)_{mix} \tag{6}$$

The Hansen solubility parameters. The Hansen solubility parameters are a way of predicting if one material will dissolve in another and form a solution. They are based on the idea that like dissolves like where one molecule is defined as being "like" another if it bonds to itself in a similar way. Specifically, each molecule is given three Hansen parameters, δ_d, δ_p, and δ_h, each generally measured in megapascal.

Flory-Huggins interaction parameter (χ). Flory-Huggins interaction parameter (χ) can be calculated from ΔE_{mix} using Eq. 7 (*42*–*44*, *62*). The smaller the Flory-Huggins parameter is, the better is the compatibility of the two components

$$\chi = \left(\frac{\Delta E_{mix}}{RT\emptyset_i\emptyset_j} \right) V_m \tag{7}$$

Fractional volume. The volume fraction (ϕ_i) of component *i* in the composite according to Eq. 8, where ρ_c is the average density, ρ_i is the density of component *i* in the composite and C_i is its concentration in wt % (*40*)

$$\phi_i = \left(\frac{C_i}{100} \right) \left(\frac{\rho_c}{\rho_i} \right) \tag{8}$$

Binding energy. The binding energy ($E_{binding}$), defined as the negative value of the interaction energy E_{inter}, is a measure of the compatibility between two components mixed with each other (*39*). A negative $E_{binding}$ represents poor compatibility between two components, while a large positive $E_{binding}$ represents good compatibility. The $E_{binding}$ between components *j* and *i* may be obtained by Eq. 9.

$$E_{binding} = -E_{Inter} = -(E_{Complex} - E_i - E_j) \tag{9}$$

Samples analysis

WAXS measurements were performed on a computer-controlled goniometer coupled with a CuKα radiation source (λ = 0.154 nm) at 30 kV and 50 mA (Panalytical B.V., Almelo, Netherlands). The analyzed samples were prepared using a compression molding procedure.

M_n, M_w, and the polydispersity index were determined using SEC. The measurements were performed at 150°C on a Polymer Char GPC-IR built around an Agilent GC oven model 7890, equipped with an autosampler and the Integrated Detector IR4. 1,2-dichlorobenzene (o-DCB) was used as an eluent at a flow rate of 1 ml min^{-1}. Polystyrene (PS) standards were selected to provide calibration points. The injection volume was 200 μl. The SEC data were processed using Calculations Software GPC One.

Melting (T_m) and crystallization (T_c) temperatures as well as enthalpies of the transitions were measured by DSC using a DSC Q100 from TA Instruments. The measurements were carried out at a heating and cooling rate of 10°C min^{-1} from −40° to 230°C under nitrogen flow (15 ml min^{-1}). The transitions were deduced from the second heating and cooling curves.

Details of the samples' morphology were examined with a transmission electron microscope (Tesla BS 500, Tesla, Czech Republic), operating at 90 kV. Samples for TEM examination, in the form of ultrathin sections approximately 60 nm thick, were prepared by cryo-ultra-sectioning with an ultramicrotome (PowerTome PC, Boeckeler, USA) equipped with a 35° diamond knife (Diatome, Switzerland). Ultrathin sections were placed on standard copper grids for TEM examination. Before cutting, the analyzed samples were exposed to the vapor of RuO_4 at room temperature for 24 hours (*63*). From TEM micrographs, the structural information on HDPE dispersion was extracted using the image analysis software ImageJ (National Institutes of Health, USA) (*64*). Size determinations were made by evaluating at least 300 domains of HDPE for each sample.

AFM was performed using the Dimension FastScan AFM system from Bruker using tapping mode AFM tips (Model TESPA-V2, k: 42 N m^{-1}, f: 320 kHz). The software NanoScope Analysis 1.5 from Bruker was used as the computer interface for the operation and analysis of AFM measurements. All AFM measurements were performed at ambient conditions. Samples were cryo-microtomed at −120°C. Height and phase images were recorded simultaneously at a scan rate of 1 Hz with a resolution of 512 × 512 pixels. Optical imaging integrated into the AFM setup was first used before AFM measurement to select the area of interest for imaging. The nanomechanical properties of the samples were characterized by a high accuracy quantitative nanomechanical mapping mode (HA-QNM) at a frequency of 0.7 Hz using TAP-150-30 silicon cantilever tips (Bruker AFM Probes, 5 N/m nominal spring constant) at ambient conditions. QNM mode enables the quantitative measurements of nanoscale material mechanical properties by performing pixel-wise force curves in the scanned area in real time. Analysis of the individual force curve data by the AFM NanoScope software provides a map of material properties with the same resolution as a topography image. Thereafter, the elastic modulus of the scanned surface was extracted from the force curve using the Derjaguin-Muller-Toropov (DMT) model and presented in the modulus mapping images.

DMTA was performed using a TA Instruments Q800 DMA. Samples were tested by a strain-controlled temperature ramp with a frequency of 1 Hz. The measurements were performed using film-tension mode. The applied temperature profile was from −150°C to the melting point of the sample with the ramp 2°C min^{-1}. The glass transition temperature was calculated as the maximum of the tangent delta signal.

Tensile tests were performed using a Zwick type Z020 tensile tester equipped with a 2.5-kN load cell according to ISO 527-3 standard (specimen type 1BA). A grip-to-grip separation of 40 mm was used. The samples were prestressed to 3 N, and then loaded with a constant cross-head speed 40 mm min^{-1}. Young's modulus was estimated with a constant cross-head speed of 1 mm min^{-1} with an external extensometer. The reported values are an average of at least 10 measurements of each composition.

A Discovery Hybrid Rheometer DHR-2 (TA instruments) equipped with a force rebalance transducer was used for the shear rheological experiments. Stainless steel 25-mm-diameter parallel plates were adopted for all the experiments. The temperature was controlled via a convection oven fed with nitrogen gas to minimize sample degradation. Samples were shaped into discotic specimens by means of hot-pressing, well above their glass transition temperature (typically at 180°C), and then cooled to room temperature. After loading, all the samples were subjected to 30 min annealing at 180°C to erase residual stresses, and to get rid of possible air bubbles, due to the hot pressing. After that, the following rheological protocol was adopted for each sample: (i) dynamic strain amplitude sweep at ω = 100 rad s^{-1} to detect the linear viscoelastic regime and (ii) dynamic frequency sweep at strain amplitudes in the range of 1 to 5% and frequency range between 100 and 0.01 rad s^{-1}.

The G-M model. According to the GM model, the frequency response of a polymer blend is given by two contributions (*54*): (i) the viscoelastic response of the individual components that constitute the dispersed and the continuous phases and (ii) the interfacial tension. Hence, the total complex shear modulus is written as Eq. 10

$$G^*_{blend} = \emptyset G^*_{PP} + (1 - \emptyset)G^*_{HDPE} + G^*_{interface} \quad (10)$$

with ϕ being the volume fraction of the dispersed phase (PP in our case), and G^*_{PP}, G^*_{HDPE}, and $G^*_{interface}$ being the complex shear modulus of the PP, HDPE, and the interfacial contribution, respectively. It is important to highlight the fact that the linear mixing rule may fail if the Newtonian viscosities of the two components are very different.

The effect of the interfacial tension on the moduli of Newtonian liquids was first addressed by Choi and Schowalter (*65*). Subsequently, in 1989, Scholz *et al.* (*66*) reported a simplified version of the previous model, where the dynamic moduli, storage (G′) and loss (G″), of a blend, can be calculated as

$$G'(\omega) = \eta\frac{\omega^2(\tau_1 - \tau_2)}{1 + \omega^2\tau_1^2} = \frac{\eta}{\tau_1}\left(1 - \frac{\tau_2}{\tau_1}\right)\frac{\omega^2\tau_1^2}{1 + \omega^2\tau_1^2} \quad (11)$$

$$G''(\omega) = \eta\frac{\omega^3\tau_1\tau_2 - \omega)}{1 + \omega^2\tau_1^2} = \frac{\eta}{\tau_1}\left(1 - \frac{\tau_2}{\tau_1}\right)\frac{\omega\tau_1}{1 + \omega^2\tau_1^2} + \omega\eta\frac{\tau_2}{\tau_1} \quad (12)$$

The parameters of the above-reported equations are defined as

$$\eta = \eta_{matrix}\left[1 + \phi\frac{(5k + 2)}{2(2k + 1)} + \phi^2\frac{5(5k + 2)^2}{8(k + 1)^2}\right] \quad (13)$$

$$\tau_1 = \tau_0\left[1 + \phi\frac{5(19k + 16)}{4(k + 1)(2k + 3)}\right] \quad (14)$$

$$\tau_2 = \tau_0\left[1 + \phi\frac{3(19k + 16)}{4(k + 1)(2k + 3)}\right] \quad (15)$$

$$\tau_0 = \frac{\eta_{matrix}R}{\alpha}\frac{(19k + 16)(2k + 3)}{40(k + 1)} \quad (16)$$

$$k = \frac{\eta_{dispersed}}{\eta_{matrix}} \quad (17)$$

where η_{matrix} and $\eta_{dispersed}$ are the Newtonian viscosities of the matrix and dispersed phase, respectively, R is the average radius of the dispersed domains, and α is the interfacial tension. It follows that the dynamic moduli of the blends are written as follows

$$G'_{blend} = \phi G'_{PP} + (1 - \phi)G'_{HDPE} + \frac{\eta}{\tau_1}\left(1 - \frac{\tau_2}{\tau_1}\right)\frac{\omega^2\tau_1^2}{1 + \omega^2\tau_1^2} \quad (18)$$

$$G''_{blend} = \phi G''_{PP} + (1 - \phi)G''_{HDPE} + \frac{\eta}{\tau_1}\left(1 - \frac{\tau_2}{\tau_1}\right)\frac{\omega\tau_1}{1 + \omega^2\tau_1^2} + \omega\eta\frac{\tau_2}{\tau_1} \quad (19)$$

Last, the complex viscosity of the resulting blend is written as

$$\eta^*_{blend} = \frac{\sqrt{G'_{blend}2 + G''_{blend}{}^2}}{\omega} \quad (20)$$

Supplementary Materials

This PDF file includes:

Supplementary Text
Figs. S1 to S22
Tables S1 to S6

REFERENCES AND NOTES

1. M. D. Tabone, J. J. Cregg, E. J. Beckman, A. E. Landis, Sustainability metrics: Life cycle assessment and green design in polymers. *Environ. Sci. Technol.* **44**, 8264–8269 (2010).
2. T. Hees, F. Zhong, M. Stürzel, R. Mülhaupt, Tailoring hydrocarbon polymers and all-hydrocarbon composites for circular economy. *Macromol. Rapid Commun.* **40**, e1800608 (2019).
3. X. Wu, A. Tennakoon, R. Yappert, M. Esveld, M. S. Ferrandon, R. A. Hackler, A. M. LaPointe, A. Heyden, M. Delferro, B. Peters, A. D. Sadow, W. Huang, Size-controlled nanoparticles embedded in a mesoporous architecture leading to efficient and selective hydrogenolysis of polyolefins. *J. Am. Chem. Soc.* **144**, 5323–5334 (2022).
4. N. M. Wang, G. Strong, V. DaSilva, L. Gao, R. Huacuja, I. A. Konstantinov, M. S. Rosen, A. J. Nett, S. Ewart, R. Geyer, S. L. Scott, D. Guironnet, Chemical recycling of polyethylene by tandem catalytic conversion to propylene. *J. Am. Chem. Soc.* **144**, 18526–18531 (2022).
5. A. Arroyave, S. Cui, J. C. Lopez, A. L. Kocen, A. M. LaPointe, M. Delferro, G. W. Coates, Catalytic chemical recycling of post-consumer polyethylene. *J. Am. Chem. Soc.* **144**, 23280–23285 (2022).
6. K. M. van Geem, Plastic waste recycling is gaining momentum. *Science* **381**, 607–608 (2023).
7. Z. Xu, N. E. Munyaneza, Q. Zhang, M. Sun, C. Posada, P. Venturo, N. A. Rorrer, J. Miscall, B. G. Sumpter, G. Liu, Chemical upcycling of polyethylene, polypropylene, and mixtures to high-value surfactants. *Science* **381**, 666–671 (2023).
8. M. Xanthos, Recycling of the #5 Polymer. *Science* **337**, 700–702 (2012).
9. K. A. Chaffin, J. S. Knutsen, P. Brant, F. S. Bates, High-strength welds in metallocene polypropylene/polyethylene laminates. *Science* **288**, 2187–2190 (2000).
10. F. C. Stehling, T. Huff, C. S. Speed, G. Wissler, Structure and properties of rubber-modified polypropylene impact blends. *J. Appl. Polym. Sci.* **26**, 2693–2711 (1981).
11. L. D'Orazio, R. Greco, E. Martuscelli, G. Ragosta, Effect of the addition of EPM copolymers on the properties of high density polyethylene/isotactic polypropylene blends: II. Morphology and mechanical properties of extruded samples. *Polym. Eng. Sci.* **23**, 489–497 (1983).
12. C. Huang, M. Olvera de la Cruz, Analytic interface profile approximation for ternary polymer blends. *Macromolecules* **29**, 6068–6070 (1996).
13. V. Busico, R. Cipullo, N. Friederichs, S. Ronca, M. Togrou, The first molecularly characterized isotactic polypropylene-block-polyethylene obtained via "quasi-living" insertion polymerization. *Macromolecules* **36**, 3806–3808 (2003).
14. V. Busico, R. Cipullo, N. Friederichs, S. Ronca, G. Talarico, M. Togrou, B. Wang, Block copolymers of highly isotactic polypropylene via controlled Ziegler-Natta polymerization. *Macromolecules* **37**, 8201–8203 (2004).
15. D. J. Arriola, E. M. Carnahan, P. D. Hustad, R. L. Kuhlman, T. T. Wenzel, Catalytic production of olefin block copolymers via chain shuttling polymerization. *Science* **312**, 714–719 (2006).
16. G. W. Coates, G. J. Domski, Pyridlyamidohafnium catalyst precursors, active species from this and uses thereof to polymerize alkenes. Patent WO2008112133A2 (2008).
17. Y. Lin, V. Yakovleva, H. Chen, A. Hiltner, E. Baer, Comparison of olefin copolymers as compatibilizers for polypropylene and high-density polyethylene. *J. Appl. Polym. Sci.* **113**, 1945–1952 (2009).
18. Y. Lin, G. R. Marchand, A. Hiltner, E. Baer, Adhesion of olefin block copolymers to polypropylene and high density polyethylene and their effectiveness as compatibilizers in blends. *Polymer (Guildf)* **52**, 1635–1644 (2011).
19. F. S. Bates, M. A. Hillmyer, T. P. Lodge, C. M. Bates, K. T. Delaney, G. H. Fredrickson, Multiblock polymers: Panacea or Pandora's box? *Science* **336**, 434–440 (2012).
20. Y. Hu, B. Conley, K. Walton, C. Shan, G. Marchand, R. Patel, K. Eva, B. Walter, Multilayered polyolefin-based films, U.S. Patent no. 9,511,567 B2 (2016).
21. K. Klimovica, S. Pan, T. W. Lin, X. Peng, C. J. Ellison, A. M. Lapointe, F. S. Bates, G. W. Coates, Compatibilization of iPP/HDPE Blends with PE-g-iPP graft copolymers. *ACS Macro Lett.* **9**, 1161–1166 (2020).
22. P. Wolff, A. Dickert, W. P. Kretschmer, R. Kempe, iPP/PE multiblock copolymers for plastic blend recycling synthesized by coordinative chain transfer polymerization. *Macromolecules* **55**, 6435–6442 (2022).
23. H. Gao, X. Lu, S. Chen, B. Du, X. Yin, Y. Kang, K. Zhang, C. Liu, L. Pan, B. Wang, Z. Ma, Y. Li, Preparation of well-controlled isotactic polypropylene-based block copolymers with superior physical performance via efficient coordinative chain transfer polymerization. *Macromolecules* **55**, 5038–5048 (2022).
24. J. M. Eagan, J. Xu, R. Di Girolamo, C. M. Thurber, C. W. Macosko, A. M. LaPointe, F. S. Bates, G. W. Coates, Combining polyethylene and polypropylene: Enhanced performance with PE/iPP multiblock polymers. *Science* **355**, 814–816 (2017).
25. M. Letizia Focarete, M. Scandola, A. Kumar, R. A. Gross, Physical characterization of poly(ω-pentadecalactone) synthesized by lipase-catalyzed ring-opening polymerization. *J Polym Sci B* **39**, 1721–1729 (2001).
26. M. De Geus, I. van der Meulen, B. Goderis, K. Van Hecke, M. Dorschu, H. van der Werff, C. E. Koning, A. Heise, Performance polymers from renewable monomers: High molecular weight poly (pentadecalactone) for fiber applications. *Polym. Chem.* **1**, 525–533 (2010).
27. F. Stempfle, P. Ortmann, S. Mecking, Long-chain aliphatic polymers to bridge the gap between semicrystalline polyolefins and traditional polycondensates. *Chem. Rev.* **116**, 4597–4641 (2016).
28. M. P. F. Pepels, R. G. Kleijnen, J. G. P. Goossens, A. B. Spoelstra, R. Tandler, H. Martens, M. Soliman, R. Duchateau, Compatibility and epitaxial crystallization between poly(ethylene) and poly(ethylene)-like polyesters. *Polymer (Guildf)* **88**, 63–70 (2016).
29. J. Panten, H. Surburg, B. Hölscher, New oxa-bridged macrocycles. *Chem. Biodivers.* **5**, 1011–1022 (2008).
30. M. P. F. Pepels, M. Bouyahyi, A. Heise, R. Duchateau, Kinetic investigation on the catalytic ring-opening (co)polymerization of (macro)lactones using aluminum salen catalysts. *Macromolecules* **46**, 4324–4334 (2013).
31. L. Jasinska-Walc, M. R. Hansen, D. Dudenko, A. Rozanski, M. Bouyahyi, M. Wagner, R. Graf, R. Duchateau, Topological behavior mimicking ethylene–hexene copolymers using branched lactones and macrolactones. *Polym. Chem.* **5**, 3306–3310 (2014).
32. L. Jasinska-Walc, M. Bouyahyi, A. Rozanski, R. Graf, M. R. Hansen, R. Duchateau, Synthetic principles determining local organization of copolyesters prepared from lactones and macrolactones. *Macromolecules* **48**, 502–510 (2015).
33. P. Gestoso, J. Brisson, Orientation of uniaxially stretched poly(vinyl phenol)/poly(vinyl methyl ether) blends. *Polymer (Guildf)* **42**, 8415–8424 (2001).
34. P. Gestoso, J. Brisson, Effect of hydrogen bonds on the amorphous phase of a polymer as determined by atomistic molecular modelling. *Comput. Theor. Polym. Sci.* **11**, 263–271 (2001).
35. M. Zhang, P. Choi, U. Sundararaj, Molecular dynamics and thermal analysis study of anomalous thermodynamic behavior of poly (ether imide)/polycarbonate blends. *Polymer (Guildf)* **44**, 1979–1986 (2003).
36. M. Tambasco, J. E. G. Lipson, J. S. Higgins, Blend miscibility and the Flory–Huggins interaction parameter: A critical examination. *Macromolecules* **39**, 4860–4868 (2006).
37. J. Gupta, C. Nunes, S. Vyas, S. Jonnalagadda, Prediction of solubility parameters and miscibility of pharmaceutical compounds by molecular dynamics simulations. *J. Phys. Chem. B* **115**, 2014–2023 (2011).
38. A. D. S. Gomes, *Polymerization* (IntechOpen, Rijeka, 2012).
39. Y. Guo, J. Liu, Y. Lu, D. Dong, W. Wang, L. Zhang, A combined molecular dynamics simulation and experimental method to study the compatibility between elastomers and resins. *RSC Adv.* **8**, 14401–14413 (2018).
40. J. L. Lebga-Nebane, M. Sankarasubramanian, G. Chojecki, B. Ning, P. A. Yuya, J. C. Moosbrugger, D. H. Rasmussen, S. Krishnan, Polyetheretherketone, hexagonal boron nitride, and tungsten carbide cobalt chromium composite coatings: Mechanical and tribological properties. *J. Appl. Polym. Sci.* **138**, 50504 (2021).
41. M. Häußler, M. Eck, D. Rothauer, S. Mecking, Closed-loop recycling of polyethylene-like materials. *Nature* **590**, 423–427 (2021).
42. H. Abou-Rachid, L.-S. Lussier, S. Ringuette, X. Lafleur-Lambert, M. Jaidann, J. Brisson, On the correlation between miscibility and solubility properties of energetic plasticizers/polymer blends: Modeling and simulation studies. *Propell. Explos.Pyrotech.* **33**, 301–310 (2008).
43. A. Ahmadi, J. J. Freire, Molecular dynamics simulation study of compatibility for the polyvinylmethylether/polystyrene mixture. *Mol. Simul.* **34**, 1253–1258 (2008).
44. X. W. Cui, L. Zhang, Amorphous state and solubility simulation of poly-(N-arylenebenzimidazole ketone). *Appl. Mech. Mater.* **513-517**, 295–298 (2014).
45. G. Natta, P. Corradini, Structure and properties of isotactic polypropylene. *Il Nuovo Cimento* **15**, 40–51 (1960).
46. M. Gazzano, V. Malta, M. L. Focarete, M. Scandola, R. A. Gross, Crystal structure of poly(ω-pentadecalactone). *J Polym Sci B* **41**, 1009–1013 (2003).
47. M. K. Mitra, M. Muthukumar, Theory of spinodal decomposition assisted crystallization in binary mixtures. *J. Chem. Phys.* **132**, 184908 (2010).
48. C. Yan, H. Li, J. Zhang, Y. Ozaki, D. Shen, D. Yan, A.-C. Shi, S. Yan, Surface-induced anisotropic chain ordering of polycarprolactone on oriented polyethylene substrate: Epitaxy and soft epitaxy. *Macromolecules* **39**, 8041–8048 (2006).
49. Z. Bartczak, A. Galeski, M. Pracella, Spherulite nucleation in blends of isotactic polypropylene with high-density polyethylene. *Polymer (Guildf)* **27**, 537–543 (1986).
50. N. W. Volchko, G. C. Rutledge, Heterogeneous nucleation of high-density polyethylene crystals on graphene within microdomains. *Macromolecules* **56**, 4123–4134 (2023).
51. R. B. Blumstein, Thermal characterization of polymeric materials. Second edition volumes 1 and 2 edited by Edith A. Turi (Polytechnic University, New York). Academic Press: San Diego. 1997. xxiv + 2420 pp. ISBN 0-12-703783-7. *J. Am. Chem. Soc.* **119**, 9589–9590 (1997).
52. M. E. Dokukin, I. Sokolov, Quantitative mapping of the elastic modulus of soft materials with HarmoniX and PeakForce QNM AFM modes. *Langmuir* **28**, 16060–16071 (2012).

53. D. Parisi, A. Han, J. Seo, R. H. Colby, Rheological response of entangled isotactic polypropylene melts in strong shear flows: Edge fracture, flow curves, and normal stresses. *J. Rheol.* **65**, 605–616 (2021).
54. H. Gramespacher, J. Meissner, Interfacial tension between polymer melts measured by shear oscillations of their blends. *J. Rheol.* **36**, 1127–1141 (1992).
55. S. Jose, A. S. Aprem, B. Francis, M. C. Chandy, P. Werner, V. Alstaedt, S. Thomas, Phase morphology, crystallisation behaviour and mechanical properties of isotactic polypropylene/high density polyethylene blends. *Eur. Polym. J.* **40**, 2105–2115 (2004).
56. J. E. Mark, *Physical Properties of Polymers Handbook*, vol. 1076 (Springer, 2007).
57. Dassault Systemes BIOVIA, Materials: Studio overview (2017).
58. D. N. Theodorou, U. W. Suter, Detailed molecular structure of a vinyl polymer glass. *Macromolecules* **18**, 1467–1478 (1985).
59. H. Sun, Ab initio characterizations of molecular structures, conformation energies, and hydrogen-bonding properties for polyurethane hard segments. *Macromolecules* **26**, 5924–5936 (1993).
60. H. Sun, COMPASS: An ab initio force-field optimized for condensed-phase applicationsoverview with details on alkane and benzene compounds. *J. Phys. Chem. B* **102**, 7338–7364 (1998).
61. M. J. McQuaid, H. Sun, D. Rigby, Development and validation of COMPASS force field parameters for molecules with aliphatic azide chains. *J. Comput. Chem.* **25**, 61–71 (2004).
62. R. L. C. Akkermans, N. A. Spenley, S. H. Robertson, COMPASS III: Automated fitting workflows and extension to ionic liquids. *Mol. Simul.* **47**, 540–551 (2021).
63. D. Montezinos, B. G. Wells, J. L. Burns, The use of ruthenium in hypochlorite as a stain for polymeric materials. *J. Polym. Sci. Polym. Lett. Ed.* **23**, 421–425 (1985).
64. National Institute of Health USA, ImageJ.
65. S. J. Choi, W. R. Schowalter, Rheological properties of nondilute suspensions of deformable particles. *Phys. Fluids* **18**, 420–427 (1975).
66. P. Scholz, D. Froelich, R. Muller, Viscoelastic properties and morphology of two-phase polypropylene/polyamide 6 blends in the Melt. Interpretation of results with an emulsion model. *J. Rheol.* **33**, 481–499 (1989).

Acknowledgments: We would like to thank H. Goossens for fruitful discussions and SABIC for the financial support. **Funding:** This project was funded by SABIC. **Author contributions:** Conceptualization: L.J.-W. and R.D. Methodology: L.J.-W. and R.D. Investigation: J.K., W.N., A.R., Y.L., D.P., L.Y., F.A.P., M.B., L.J.-W., and R.D. Visualization: J.K., W.N., D.P., F.A.P., L.J.-W., and R.D. Funding acquisition: L.J.-W. and R.D. Project administration: L.J.-W. and R.D. Supervision: L.J.-W. and R.D. Writing—original draft: L.J.-W., R.D., D.P., and F.A.P. Writing—review and editing: L.J.-W. and R.D. **Competing interests:** Parts of this work have been described in a patent application: WO2016188817A1. The authors declare that they have no other competing interests. **Data and materials availability:** All data needed to evaluate the conclusions in the paper are present in the paper and/or the Supplementary Materials.

Submitted 21 January 2024
Accepted 17 April 2024
Published 23 May 2024
10.1126/sciadv.ado1944